

PHASE RETRIEVAL FOR RYDBERG QUANTUM ARRAYS

*Peter Vouras[†], Kumar Vijay Mishra[‡], Alexandra Artusio-Glimpse**

[†]United States Department of Defense, Washington, DC, 20375 USA

[‡]United States DEVCOM Army Research Laboratory, Adelphi, MD 20783 USA

*National Institute of Standards and Technology, Boulder, CO, 80303 USA

ABSTRACT

In this paper we derive a novel phase retrieval algorithm for use in phased array or synthetic aperture applications where only measurements of electric field intensity are possible at each spatial sample. Such array configurations exist if a Rydberg atom probe is used in place of an antenna. We present outcomes of numerical experiments showing the effectiveness of the proposed algorithm.

Index Terms— phase retrieval, quantum synthetic apertures, Rydberg sensing

1. INTRODUCTION

Phase retrieval is the process of recovering a signal from the magnitude of its Fourier transform. This problem has been studied in a number of applications, such as optics [1], X-ray crystallography [2, 3], speech recognition [4], blind channel estimation [5], and astronomy [6]. The interest in phase retrieval is largely due to the inability of a sensing device to measure the phase of a received signal. For one-dimensional (1D) signals, the problem is ill-posed, meaning more than one signal with different phase can map to the same magnitude; the only exceptions being a minimum-phase signal [7] or a sparse signal with structured support [8]. Substantial work has been done and is still ongoing to overcome the ill-posedness of the problem, and the literature is too large to summarize here (e.g. see [9, 10] for contemporary surveys, and references therein). Overall, two major approaches have emerged: the first harnesses prior knowledge of the signal structure, such as sparse support [11–13], while the other exploits technology to make additional measurements of the magnitude via, for example, masks [14] and short-time Fourier transform (STFT) [15–17].

Recent work at the National Institute of Standards and Technology (NIST) and many other institutions has demonstrated the feasibility of using Rydberg atom probes to provide traceable measurements of electric field intensity [18]. These quantum probes have many unique features that set them apart from traditional antennas including exactly defined response functions based on quantum mechanics allowing for direct field strength traceability to the International System of Units (SI) [19–23], a highly transparent probe head to RF fields made only of dielectric materials [24, 25], direct down-conversion of the RF field by the atoms reducing the need for back-end electronics [26], and intrinsic ultra-wideband tunability from kilohertz frequencies to terahertz frequencies using a single probe and a tunable laser [21, 27]. These unique features have

attracted a large number of RF scientists, engineers, and developers to these Rydberg atom probes; however, one limitation of these probes is in the detection of phase. Typically, in order to resolve the phase of the incident RF field, a second RF field acting as a local-oscillator (LO) is radiated onto the Rydberg atom probe [28, 29]. The radiated LO has implications for the transparency of the probe because it requires an additional antenna as well as impacting the usefulness of these probes in stealth applications. One alternative phase sensing approach has been put forward [30] wherein an optical LO is used rather than a radiated RF LO; however, this scheme is limited to sensing only a single quadrant of phase space because it is essentially still an intensity detector. Thus, processing schemes that recover phase information from a purely intensity set of measurements are of interest for applications that use the Rydberg atom probes in a synthetic aperture measurement (e.g. [24, 31]).

The algorithm described in this paper is intended to retrieve an estimate of signal phase from intensity-only measurements such that the Rydberg atom probe can be used to construct a synthetic aperture. Synthetic apertures increase the effective area, and thereby angular resolution, of an imaging system beyond the physical limits of a hardware antenna. A synthetic aperture is constructed by using a mechanical positioner to move a measurement probe or antenna through space. The probe measures at discrete locations the RF fields propagating across the aperture and if the spatial RF samples maintain phase coherence then they can be combined in post-processing to create high-resolution snapshots of the ambient scattering.

2. MEASUREMENT MODEL

The Rydberg atom probe measurement utilizes sensitive Rydberg states (high energy states where the electron of an alkali atom is far from and weakly coupled to the nucleus) to detect RF electric fields. These Rydberg states are reached using a set of lasers. A near-infrared probe laser couples to the ground state of the atoms and is detected with a photodetector after passing through the atomic vapor cell, as depicted in Fig. 1. Because the probe laser is resonant with ground states of the atoms, this laser is preferentially absorbed and minimal light reaches the photodetector. Then, a counter-propagating visible coupling laser excites the atoms to a Rydberg state where the principle quantum number is large and the energy separation between adjacent Rydberg states is small (e.g. on the order of RF frequencies). The combination of these two lasers produces an effect known as electromagnetically induced transparency (EIT), wherein the atoms become transparent to the probe laser over a narrow frequency range and the light reaching the detector increases, see Fig. 2. When the atoms are then radiated by an RF field that is resonant with a second Rydberg state, the narrow EIT line

K. V. M. acknowledges support from the National Academies of Sciences, Engineering, and Medicine via Army Research Laboratory Harry Diamond Distinguished Fellowship.

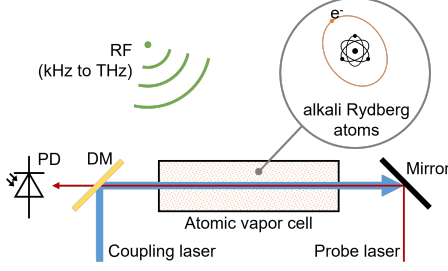


Fig. 1: Diagram of the Rydberg atom electric field measurement setup. PD is a photodetector and DM is a dichroic mirror. This same set of hardware can be used to detect RF electric fields from kHz to THz.

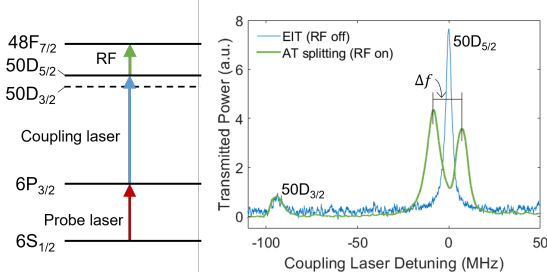


Fig. 2: Example Rydberg measurement when a 26.105 GHz RF field radiates ^{85}Rb atoms excited to the $50D_{5/2}$ Rydberg state by the probe laser (resonant with the $6S_{1/2}$ and $6P_{3/2}$ states) and the coupling laser (resonant with the $6P_{3/2}$ and $50D_{5/2}$ states). When the coupling laser frequency is detuned, the EIT line of the probe transmittance appears (blue line). When the coupling laser is far detuned in the negative frequency direction, another weaker EIT line appears from the $50D_{3/2}$ state, which is used to calibrate the frequency axis of the spectrum. Once the resonant RF field is turned on, the main EIT line splits (green line) and the frequency difference, Δ_f , is directly proportional to the field strength of the RF and the dipole moment of the $50D_{5/2}$ to $48F_{7/2}$ transition, Eq. 1.

splits known as Autler-Townes (AT) splitting. The frequency difference of this AT line splitting, Δ_f , is proportional to the absolute value of the electric field of the RF, $|E_{RF}|$:

$$\Delta_f = \frac{\varphi}{h} |E_{RF}|, \quad (1)$$

where φ is the dipole moment of the Rydberg transition, which is accurately calculated [32], and $h = 6.62607015 \times 10^{-34} \text{ J Hz}^{-1}$ is Planck's constant, a fundamental unit in the new SI. Once the on-resonance (detuning of 0 MHz in Fig. 2) change in probe laser transmittance with RF field strength is calibrated, both laser frequencies can be locked and fast sensing of the RF field can be achieved. Our paper considers this Rydberg atom RF field measurement system when the sensor, the vapor cell and lasers packed with fiber-coupling [24], is scanned over a spatial plane defining a synthetic aperture and measurements of the RF electric field intensity are captured at each location. Due to the absolute value in Eq. 1, no phase information of the RF field is captured and must be retrieved using the processing described below.

A common approximation, also used here, is that signal sources in the scene are far enough away from the observation plane of the aperture that the impinging phase front is nearly planar. An additional assumption is that the signal is narrowband, e.g. a sinusoidal tone. With these conditions satisfied, a linear signal model describes

the signals propagating across an array of N elements as a sum of plane waves, or $\mathbf{A}\mathbf{s} = \mathbf{b}$.

The columns of \mathbf{A} are steering vectors sampled on a discrete search grid of K angles (u_i, v_i) defined in sine space coordinates,

$$\mathbf{A} = [\mathbf{a}(u_0, v_0) \quad \dots \quad \mathbf{a}(u_{K-1}, v_{K-1})] \quad (2)$$

with

$$\mathbf{a}(u_i, v_i) = [e^{jk(x_0 u_i + y_0 v_i)} \quad \dots \quad e^{jk(x_{N-1} u_i + y_{N-1} v_i)}]^T. \quad (3)$$

The vector \mathbf{s} contains the (unknown) complex signal source amplitudes and the vector \mathbf{b} represents the complex output of the array or synthetic aperture. The probe measures intensity or $|\mathbf{b}_k|^2$ at the k th spatial sample in the aperture. The N rows of \mathbf{A} are electrical angle vectors that specify all possible phases at each array element over all angles in the search grid,

$$\mathbf{A} = [\mathbf{f}_1^T \quad \dots \quad \mathbf{f}_{N-1}^T]^T. \quad (4)$$

For example,

$$\mathbf{f}_i = [e^{jk(x_i u_0 + y_i v_0)} \quad \dots \quad e^{jk(x_i u_{K-1} + y_i v_{K-1})}]^T. \quad (5)$$

Since the probe measures electric field intensity at each array element,

$$|\mathbf{b}_k|^2 \equiv b_k^2 = | \langle \mathbf{f}_k, \mathbf{s} \rangle |^2 = | \mathbf{f}_k^H \mathbf{s} |^2. \quad (6)$$

The objective function to optimize is the maximum error between the intensity measurements and the magnitude squared signal model,

$$\text{minimize} \max_k | |\mathbf{b}_k|^2 - | \mathbf{A}\mathbf{s} |_k^2 | \quad (7)$$

or equivalently,

$$\text{minimize} \max_k | b_k^2 - | \mathbf{f}_k^H \mathbf{s} |^2 | \quad (8)$$

for $k = 0, \dots, N-1$. This objective can be restated as

$$\text{minimize} \quad \delta \quad (9)$$

$$\text{subject to} \quad | | \mathbf{f}_0^H \mathbf{s} |^2 - b_0^2 | \leq \delta$$

\vdots

$$| | \mathbf{f}_{N-1}^H \mathbf{s} |^2 - b_{N-1}^2 | \leq \delta$$

$$\delta \geq 0.$$

Rearranging and expanding terms yields,

$$\text{minimize} \quad \delta \quad (10)$$

$$\text{subject to} \quad \mathbf{s}^H \mathbf{f}_0 \mathbf{f}_0^H \mathbf{s} - \delta \leq b_0^2, \quad -\mathbf{s}^H \mathbf{f}_0 \mathbf{f}_0^H \mathbf{s} - \delta \leq -b_0^2,$$

\vdots

$$\mathbf{s}^H \mathbf{f}_{N-1} \mathbf{f}_{N-1}^H \mathbf{s} - \delta \leq b_{N-1}^2, \quad -\mathbf{s}^H \mathbf{f}_{N-1} \mathbf{f}_{N-1}^H \mathbf{s} - \delta \leq -b_{N-1}^2,$$

$$\delta \geq 0.$$

Using the matrix trace results in,

$$\text{minimize} \quad \delta \quad \text{subject to} \quad (11)$$

$$\text{Tr} [\mathbf{f}_0 \mathbf{f}_0^H \mathbf{s} \mathbf{s}^H] - \delta \leq b_0^2, \quad -\text{Tr} [\mathbf{f}_0 \mathbf{f}_0^H \mathbf{s} \mathbf{s}^H] - \delta \leq -b_0^2,$$

\vdots

$$\text{Tr} [\mathbf{f}_{N-1} \mathbf{f}_{N-1}^H \mathbf{s} \mathbf{s}^H] - \delta \leq b_{N-1}^2,$$

$$-\text{Tr} [\mathbf{f}_{N-1} \mathbf{f}_{N-1}^H \mathbf{s} \mathbf{s}^H] - \delta \leq -b_{N-1}^2,$$

$$\delta \geq 0.$$

To relax the constraints replace the rank-one matrix $\mathbf{s} \mathbf{s}^H$ with the matrix \mathbf{S} of general rank. Applying this change and using the sub-

stitution $\text{Tr}[\mathbf{A}^H \mathbf{B}] = \text{vec}(\mathbf{A})^H \text{vec}(\mathbf{B})$ yields,

$$\begin{aligned} & \text{minimize } \delta \\ & \text{subject to } [\widehat{\mathbf{A}}\widehat{\mathbf{s}}]_k - \delta \leq b_k^2 \quad k = 0, \dots, N-1 \\ & \quad - [\widehat{\mathbf{A}}\widehat{\mathbf{s}}]_k - \delta \leq -b_k^2 \quad k = 0, \dots, N-1 \\ & \quad \delta \geq 0 \end{aligned} \quad (12)$$

where $\widehat{\mathbf{s}} = \text{vec}(\mathbf{S})$ and

$$\widehat{\mathbf{A}} = \begin{bmatrix} \text{vec}(\mathbf{f}_0 \mathbf{f}_0^H)^T & & \\ & \dots & \\ & & \text{vec}(\mathbf{f}_{N-1} \mathbf{f}_{N-1}^H)^T \end{bmatrix}^T. \quad (13)$$

We can write this objective in the form of a standard linear program as

$$\begin{aligned} & \text{minimize } [0 \ 0 \ \dots \ 1] \begin{bmatrix} \widehat{\mathbf{s}} \\ \delta \end{bmatrix} \\ & \text{subject to } \begin{bmatrix} \widehat{\mathbf{A}} & -1 \\ -\widehat{\mathbf{A}} & -1 \end{bmatrix} \begin{bmatrix} \widehat{\mathbf{s}} \\ \delta \end{bmatrix} \leq \begin{bmatrix} \mathbf{b}^2 \\ -\mathbf{b}^2 \end{bmatrix} \\ & \quad \delta \geq 0. \end{aligned} \quad (14)$$

Define the matrices

$$\begin{aligned} \overline{\mathbf{A}} &= \begin{bmatrix} \Re(\widehat{\mathbf{A}}) & -\Im(\widehat{\mathbf{A}}) \\ \Im(\widehat{\mathbf{A}}) & \Re(\widehat{\mathbf{A}}) \end{bmatrix}, \\ \overline{\mathbf{b}} &= \begin{bmatrix} \mathbf{b}^2 \\ \mathbf{0} \end{bmatrix}, \quad \overline{\mathbf{s}} = \begin{bmatrix} \Re(\widehat{\mathbf{s}}) \\ \Im(\widehat{\mathbf{s}}) \end{bmatrix}. \end{aligned} \quad (15)$$

Then the final optimization program takes the form,

$$\begin{aligned} & \text{minimize } [0 \ 0 \ \dots \ 1] \begin{bmatrix} \overline{\mathbf{s}} \\ \delta \end{bmatrix} \\ & \text{subject to } \begin{bmatrix} \overline{\mathbf{A}} & -1 \\ -\overline{\mathbf{A}} & -1 \end{bmatrix} \begin{bmatrix} \overline{\mathbf{s}} \\ \delta \end{bmatrix} \leq \begin{bmatrix} \overline{\mathbf{b}} \\ -\overline{\mathbf{b}} \end{bmatrix} \\ & \quad \delta \geq 0. \end{aligned} \quad (16)$$

A regularization term to encourage a sparse solution can be added to the objective function as in

$$\begin{aligned} & \text{minimize } [0 \ 0 \ \dots \ 1] \begin{bmatrix} \overline{\mathbf{s}} \\ \delta \end{bmatrix} + \left\| \begin{bmatrix} \overline{\mathbf{s}} \\ \delta \end{bmatrix} \right\|_1 \\ & \text{subject to } \begin{bmatrix} \overline{\mathbf{A}} & -1 \\ -\overline{\mathbf{A}} & -1 \end{bmatrix} \begin{bmatrix} \overline{\mathbf{s}} \\ \delta \end{bmatrix} \leq \begin{bmatrix} \overline{\mathbf{b}} \\ -\overline{\mathbf{b}} \end{bmatrix} \\ & \quad \delta \geq 0. \end{aligned} \quad (17)$$

This program can be solved using interior point methods and optimization toolboxes such as CVX. Once the complex matrix \mathbf{S} has been reconstructed from the solution $\overline{\mathbf{s}}$, it is still necessary to determine the best rank-one approximation \mathbf{s}_{opt} to \mathbf{S} . One can refer to [33] for a proof that

$$\mathbf{s}_{opt} = (\mathbf{v}^H \mathbf{S} \mathbf{v}) \mathbf{v} \mathbf{v}^H \quad (18)$$

where \mathbf{v} is the eigenvector of \mathbf{S} corresponding to the largest eigenvalue. Next, the final vector of complex signal source coefficients is used to determine the corresponding array output vector $\mathbf{b}_{est} = \mathbf{A} \mathbf{s}_{opt}$. In the second and third stages of the algorithm described in Section 3, alternating projections between the sets of feasible signal sources and array output magnitudes are used to search for $e^{-j\angle \mathbf{b}}$.

3. ALTERNATING PROJECTIONS

The second stage of the alternating projections algorithm is a projection into the set of feasible signal sources. To implement this projection it is necessary to estimate or know the number of signal

sources \widehat{K} apriori. Define the matrices,

$$\begin{aligned} \widetilde{\mathbf{A}} &= \begin{bmatrix} \Re(\mathbf{A}) & -\Im(\mathbf{A}) \\ \Im(\mathbf{A}) & \Re(\mathbf{A}) \end{bmatrix}, \\ \widetilde{\mathbf{b}} &= \begin{bmatrix} \Re(\mathbf{b}_{est}) \\ \Im(\mathbf{b}_{est}) \end{bmatrix}, \quad \widetilde{\mathbf{s}} = \begin{bmatrix} \Re(\mathbf{s}) \\ \Im(\mathbf{s}) \end{bmatrix}. \end{aligned} \quad (19)$$

We can solve the lower-dimension linear program for $\widetilde{\mathbf{s}}$,

$$\begin{aligned} & \text{minimize } [0 \ 0 \ \dots \ 1] \begin{bmatrix} \widetilde{\mathbf{s}} \\ \delta \end{bmatrix} \\ & \text{subject to } \begin{bmatrix} \widetilde{\mathbf{A}} & -1 \\ -\widetilde{\mathbf{A}} & -1 \end{bmatrix} \begin{bmatrix} \widetilde{\mathbf{s}} \\ \delta \end{bmatrix} \leq \begin{bmatrix} \widetilde{\mathbf{b}} \\ -\widetilde{\mathbf{b}} \end{bmatrix}, \quad \delta \geq 0. \end{aligned} \quad (20)$$

The projection onto the set of feasible signal sources is implemented by retaining the \widehat{K} largest coefficients $\{\widetilde{s}_0, \widetilde{s}_1, \dots, \widetilde{s}_{\widehat{K}-1}\}$ of $\widetilde{\mathbf{s}}$ as in

$$\mathbf{s}_{proj} = [\widetilde{s}_0 \ \widetilde{s}_1 \ \dots \ \widetilde{s}_{\widehat{K}-1} \ 0 \ \dots \ 0]^T. \quad (21)$$

A new estimate of the array output vector is

$$\mathbf{b}_1 = |\mathbf{b}| \odot e^{-j\angle \mathbf{A} \mathbf{s}_{proj}}. \quad (22)$$

Algorithm 1 Three-Stage Phase Retrieval Algorithm

STAGE 1: COMPUTING INITIAL CONDITIONS

- 1: Construct a dense uniformly sampled grid of L angles; $\{(u_l, v_l) \mid l = 0, \dots, L-1\}$. Use this grid to create the array manifold matrix \mathbf{A} given in (2).
- 2: Solve the optimization program in (17) for $\overline{\mathbf{s}}$ and rearrange the result to obtain \mathbf{S} . Use (18) to obtain \mathbf{s}_{opt} from \mathbf{S} .
- 3: Compute the corresponding array output vector $\mathbf{b}_{est} = \mathbf{A} \mathbf{s}_{opt}$.
- 4: Set the initial complex array output estimate to $\mathbf{b}_0^\dagger = |\mathbf{b}| \odot e^{-j\angle \mathbf{b}_{est}}$. This step effectively projects the vector \mathbf{b}_{est} onto the set of feasible array output magnitudes.

STAGE 2: LINEAR PROGRAM

- 1: Use \mathbf{b}_{est} to create the vector $\overline{\mathbf{b}}$ in (19).
- 2: Solve the linear program in (20) for $\overline{\mathbf{s}}$ and retain the \widehat{K} -largest coefficients as in (21) to create the vector \mathbf{s}_{proj} .
- 3: Update the complex array output estimate to $\mathbf{b}_1^\dagger = \mathbf{b}_0^\dagger \odot e^{-j\angle \mathbf{A} \mathbf{s}_{proj}}$.

STAGE 3: CONJUGATE GRADIENT ITERATIONS

- 1: Create the matrix $\mathbf{R} = \mathbf{b}_1^\dagger \mathbf{b}_1^{H\dagger} + \nu \mathbf{I}$ for small $\nu > 0$.
 - 2: Initialize the conjugate gradient algorithm with $\mathbf{w}_0 = e^{-j\angle \mathbf{A} \mathbf{s}_{proj}}$.
 - 3: Set $\mathbf{g}_0 = \mathbf{h}_0 = \nabla P(\mathbf{w}_0)$.
 - 4: For $k = 0, 1, \dots, J-1$ iterations compute t_k such that $P(e^{-jt_k \text{Diag}[\mathbf{h}_k]} \mathbf{w}_k) \geq P(e^{-jt \text{Diag}[\mathbf{h}_k]} \mathbf{w}_k) \forall t \geq 0$.
 - 5: Set $\mathbf{w}_{k+1} = e^{-jt_k \text{Diag}[\mathbf{h}_k]} \mathbf{w}_k$.
 - 6: Set $\mathbf{g}_{k+1} = \nabla P(\mathbf{w}_{k+1})$.
 - 7: Set $\mathbf{h}_{k+1} = \mathbf{g}_{k+1} + \gamma_k \mathbf{h}_k$, $\gamma_k = \frac{(\mathbf{g}_{k+1} - \mathbf{g}_k)^T \mathbf{g}_{k+1}}{\|\mathbf{g}_k\|^2}$.
 - 8: After N_{cg} gradient iterations set $\mathbf{b}_{est} = \mathbf{b}_0^\dagger = |\mathbf{b}| \odot e^{-j\angle \mathbf{w}_{cg}}$ and return to Step 1 in Stage 2 for the next linear program iteration.
 - 9: After executing Stage 2 and Stage 3 for N_{ap} iterations the final solution is $|\mathbf{b}| \odot e^{-j\angle \mathbf{w}_{ap}}$.
-

We now seek to maximize the array output power,

$$P(\mathbf{w}) = |\mathbf{w}^H \mathbf{b}_1|^2 = \mathbf{w}^H \mathbf{b}_1 \mathbf{b}_1^H \mathbf{w} \equiv \mathbf{w}^H \mathbf{R} \mathbf{w} \quad (23)$$

where \mathbf{w} is a vector of phase weights,

$$\mathbf{w} = [e^{j\phi_0} \ e^{j\phi_1} \ \dots \ e^{j\phi_{N-1}}]^T. \quad (24)$$

The gradient vector $\nabla P(\mathbf{w})$ can be computed using an approach described in [34] as,

$$\nabla P(\mathbf{w}) = \frac{1}{\mathbf{w}^H \mathbf{w}} \Im(\text{diag}[\mathbf{R} - P_s(\mathbf{w})\mathbf{I}, \mathbf{w}\mathbf{w}^H]), \quad (25)$$

where $[\mathbf{A}, \mathbf{B}] = \mathbf{A}\mathbf{B} - \mathbf{B}\mathbf{A}$. Conjugate gradient iterations can now be used to find an optimal solution for \mathbf{w} .

In the algorithm, notice that the input to Stage 2 from Stage 3, $|\mathbf{b}| \odot e^{-j\angle \mathbf{w}_{cg}}$, is a projection onto the set of feasible array output magnitudes. Likewise, the pruning operation in Step 2 of Stage 2 to create \mathbf{s}_{proj} is a projection onto the set of feasible signal sources. Thus the algorithm alternates projections between two constraint sets. The primary purpose of Stage 1 is to provide a reliable and consistent starting point for the alternating projections.

4. NUMERICAL EXPERIMENTS

This section provides simulation results that demonstrate the phase retrieval algorithm. Two signal sources of 10 and 8 dB are located at coordinates (-1663, 3155, 2870) and (1301, 2878, 0), in units of mm, with respect to a planar 7-by-7 synthetic aperture centered at the origin. The spacing between spatial samples of the synthetic aperture is $\lambda/2$ at 40 GHz. The total signal received at the m th spatial sample of the synthetic aperture is given by

$$y_m = \sum_{k=0}^{\hat{K}-1} \sqrt{P_k} e^{j(2\pi/\lambda)d_{km}} \quad (26)$$

where P_k is the signal power and d_{km} is the distance from the k th signal source to the m th spatial sample in the aperture. In this scenario, the number of signal sources $\hat{K} = 2$. Fig. 3 illustrates the ground truth beamformed output created with perfect knowledge of the phase. Fig. 4 illustrates the beamformed output when electric field intensity is measured and the phase is estimated. The results show agreement between the estimated and true signal sources within one beamwidth. Fig. 5 illustrates the true and estimated unwrapped phase modulo 2π across the spatial samples of the synthetic aperture. Fig. 6 illustrates the progression of the scalar δ from (20).

5. SUMMARY

In this paper a novel alternating projections algorithm is derived for estimating signal phase at each spatial sample of a synthetic aperture where the receive probe is a Rydberg quantum sensor that measures electric field intensity.

6. REFERENCES

- [1] A. Walther, "The question of phase retrieval in optics," *Journal of Modern Optics*, vol. 10, no. 1, pp. 41–49, 1963.
- [2] R. W. Harrison, "Phase problem in crystallography," *Journal of the Optical Society of America*, vol. 10, no. 5, pp. 1046–1055, 1993.
- [3] R. P. Millane, "Phase retrieval in crystallography and optics," *Journal of the Optical Society of America*, vol. 7, no. 3, pp. 394–411, 1990.
- [4] L. Rabiner and B.-H. Juang, *Fundamentals of speech recognition*. Prentice Hall, 1993.
- [5] B. Baykal, "Blind channel estimation via combining autocorrelation and blind phase estimation," *IEEE Transactions on Circuits and Systems I: Regular Papers*, vol. 51, no. 6, pp. 1125–1131, 2004.

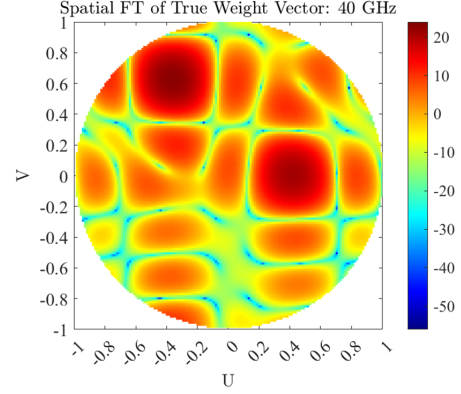


Fig. 3: Beamformed array output with known phase information

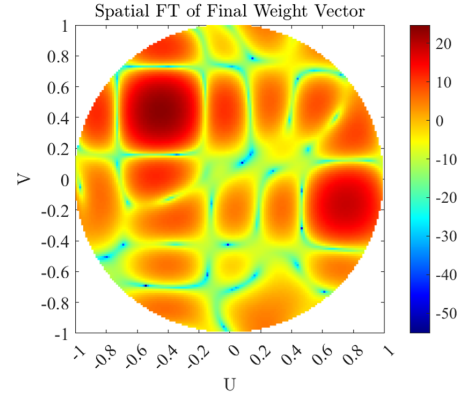


Fig. 4: Beamformed array output after estimating phase

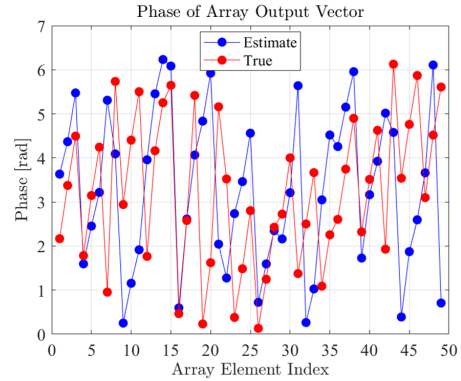


Fig. 5: True versus estimated phase across aperture

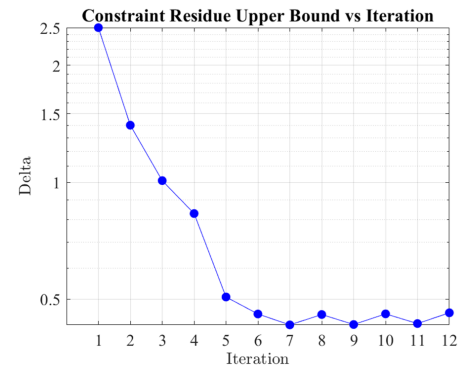


Fig. 6: Decreasing upper bound on maximum magnitude error (denoted as δ in the text)

- [6] J. C. Fienup and J. R. Dainty, "Phase retrieval and image reconstruction for astronomy," in *Image Recovery: Theory and Application*, H. Stark, Ed. Academic Press, 1987, pp. 231–275.
- [7] K. Huang, Y. C. Eldar, and N. D. Sidiropoulos, "Phase retrieval from 1d fourier measurements: Convexity, uniqueness, and algorithms," *arXiv preprint arXiv:1603.05215*, 2016.
- [8] J. Ranieri, A. Chebira, Y. M. Lu, and M. Vetterli, "Phase retrieval for sparse signals: Uniqueness conditions," *arXiv preprint arXiv:1308.3058*, 2013.
- [9] Y. Shechtman, Y. C. Eldar, O. Cohen, H. N. Chapman, J. Miao, and M. Segev, "Phase retrieval with application to optical imaging: A contemporary overview," *IEEE Signal Processing Magazine*, vol. 32, no. 3, pp. 87–109, 2015.
- [10] K. Jaganathan, Y. C. Eldar, and B. Hassibi, "Phase retrieval: An overview of recent developments," *arXiv preprint arXiv:1510.07713*, 2015.
- [11] Y. Shechtman, Y. C. Eldar, A. Szameit, and M. Segev, "Sparsity based sub-wavelength imaging with partially incoherent light via quadratic compressed sensing," *Optics Express*, vol. 19, no. 16, pp. 14 807–14 822, 2011.
- [12] K. Jaganathan, S. Oymak, and B. Hassibi, "Sparse phase retrieval: Uniqueness guarantees and recovery algorithms," *arXiv preprint arXiv:1311.2745*, 2013.
- [13] Y. Shechtman, A. Beck, and Y. C. Eldar, "GESPAR: Efficient phase retrieval of sparse signals," *IEEE Transactions on Signal Processing*, vol. 62, no. 4, pp. 928–938, 2014.
- [14] E. J. Candès, X. Li, and M. Soltanolkotabi, "Phase retrieval from coded diffraction patterns," *Applied and Computational Harmonic Analysis*, vol. 39, no. 2, pp. 277–299, 2015.
- [15] Y. C. Eldar, P. Sidorenko, D. G. Mixon, S. Barel, and O. Cohen, "Sparse phase retrieval from short-time Fourier measurements," *IEEE Signal Processing Letters*, vol. 22, no. 5, pp. 638–642, 2015.
- [16] K. Jaganathan, Y. C. Eldar, and B. Hassibi, "STFT phase retrieval: Uniqueness guarantees and recovery algorithms," *IEEE Journal of Selected Topics in Signal Processing*, vol. 10, no. 4, pp. 770–781, 2016.
- [17] T. Bendory and Y. C. Eldar, "Non-convex phase retrieval from stft measurements," *arXiv preprint arXiv:1607.08218*, 2016.
- [18] A. Artusio-Glimpse, M. T. Simons, N. Prajapati, and C. L. Holloway, "Modern rf measurements with hot atoms: A technology review of rydberg atom-based radio frequency field sensors," *IEEE Microwave Magazine*, vol. 23, no. 5, pp. 44–56, 2022.
- [19] J. A. Gordon, C. L. Holloway, S. Jefferts, and T. Heavenr, "Quantum-based si traceable electric-field probe," in *2010 IEEE International Symposium on Electromagnetic Compatibility*, 2010, pp. 321–324.
- [20] J. A. Sedlacek, A. Schwettmann, H. Kübler, R. Löw, T. Pfau, and J. P. Shaffer, "Microwave electrometry with Rydberg atoms in a vapour cell using bright atomic resonances," *Nature Physics*, vol. 8, no. 11, pp. 819–824, Nov. 2012.
- [21] C. L. Holloway, J. A. Gordon, S. Jefferts, A. Schwarzkopf, D. A. Anderson, S. A. Miller, N. Thaicharoen, and G. Raithel, "Broadband rydberg atom-based electric-field probe for si-traceable, self-calibrated measurements," *IEEE Transactions on Antennas and Propagation*, vol. 62, no. 12, pp. 6169–6182, 2014.
- [22] J. A. Gordon, C. L. Holloway, A. Schwarzkopf, D. A. Anderson, S. Miller, N. Thaicharoen, and G. Raithel, "Millimeter wave detection via autler-townes splitting in rubidium rydberg atoms," *Applied Physics Letters*, vol. 105, no. 2, p. 024104, 2014. [Online]. Available: <https://doi.org/10.1063/1.4890094>
- [23] D. A. Anderson, R. E. Sapiro, and G. Raithel, "A self-calibrated si-traceable rydberg atom-based radio frequency electric field probe and measurement instrument," *IEEE Transactions on Antennas and Propagation*, vol. 69, no. 9, pp. 5931–5941, 2021.
- [24] M. T. Simons, J. A. Gordon, and C. L. Holloway, "Fiber-coupled vapor cell for a portable rydberg atom-based radio frequency electric field sensor," *Appl. Opt.*, vol. 57, no. 22, pp. 6456–6460, Aug 2018. [Online]. Available: <http://www.osapublishing.org/ao/abstract.cfm?URI=ao-57-22-6456>
- [25] D. A. Anderson, G. A. Raithel, E. G. Paradis, and R. E. Sapiro, "Atom-based electromagnetic field sensing element and measurement system," *Application 17/838 954*, 2022.
- [26] C. L. Holloway, M. T. Simons, A. H. Haddab, C. J. Williams, and M. W. Holloway, "A "real-time" guitar recording using rydberg atoms and electromagnetically induced transparency: Quantum physics meets music," *AIP Advances*, vol. 9, no. 6, p. 065110, 2019. [Online]. Available: <https://doi.org/10.1063/1.5099036>
- [27] D. H. Meyer, P. D. Kunz, and K. C. Cox, "Waveguide-coupled rydberg spectrum analyzer from 0 to 20 ghz," *Phys. Rev. Applied*, vol. 15, p. 014053, Jan 2021. [Online]. Available: <https://link.aps.org/doi/10.1103/PhysRevApplied.15.014053>
- [28] M. T. Simons, A. H. Haddab, J. A. Gordon, and C. L. Holloway, "A rydberg atom-based mixer: Measuring the phase of a radio frequency wave," *Applied Physics Letters*, vol. 114, no. 11, p. 114101, 2019.
- [29] M. Jing, Y. Hu, J. Ma, H. Zhang, L. Zhang, L. Xiao, and S. Jia, "Atomic superheterodyne receiver based on microwave-dressed Rydberg spectroscopy," *Nature Physics*, vol. 16, no. 9, pp. 911–915, Jun. 2020.
- [30] D. Anderson, R. Sapiro, L. Gonçalves, R. Cardman, and G. Raithel, "Optical radio-frequency phase measurement with an internal-state rydberg atom interferometer," *Phys. Rev. Applied*, vol. 17, p. 044020, Apr 2022. [Online]. Available: <https://link.aps.org/doi/10.1103/PhysRevApplied.17.044020>
- [31] R. Cardman, L. F. Gonçalves, R. E. Sapiro, G. Raithel, and D. A. Anderson, "Atomic 2d electric field imaging of a yagi-uda antenna near-field using a portable rydberg-atom probe and measurement instrument," *Advanced Optical Technologies*, vol. 9, no. 5, 2020.
- [32] M. T. Simons, J. A. Gordon, and C. L. Holloway, "Simultaneous use of cs and rb rydberg atoms for dipole moment assessment and rf electric field measurements via electromagnetically induced transparency," *Journal of Applied Physics*, vol. 120, no. 12, p. 123103, 2016.
- [33] C. R. J. Roger A. Horn, *Matrix Analysis*. Cambridge University Press, 1999.
- [34] S. T. Smith, "Optimum phase-only adaptive nulling," *IEEE Transactions on Signal Processing*, vol. 47, no. 7, pp. 1835–1843, 1999.